In particular, the FEL has derivatives with respect to the detuning parameter. This is due to the differences between stimulated emission (gain proportional to inversion) and stimulated scattering (gain proportional to slope of distribution). Thus in the optical problem the magnitude of the vector (i.e., $u^2 + v^2 + w^2$) is conserved for all δ, while in the FEL only $\int (w_1^2 + w_2^2 + w_3^2)\, d\mu$ is conserved.

We examine the case of "photon echo" to see whether there are coherent phenomena in the FEL analogous to those in the coherent optical problem and NMR. We suppose that three regions of helical magnetic field are separated by drift regions in which the bunched electrons dephase as they move through in free flight. The electrons exit from the first magnet at $z = 0$ and pass through a short "phase inverting" magnet between $z = z_1$ and $z = z_1 + \Delta z$. We consider where to locate a third magnet section so as to observe emission from a phased array of dipoles. Inside the phase inverter, we neglect the effects of the dephasing terms $-\mu w_2$ and μw_1 in Eqs. (6) and (7). Then the effect of the phase inverter on (w_1, w_2, w_3) may be represented by the operator matrix

$$\begin{pmatrix} \cosh(\theta_1 \partial/\partial\mu) & 0 & \sinh(\theta_1 \partial/\partial\mu) \\ 0 & 1 & 0 \\ \sinh(\theta_1 \partial/\partial\mu) & 0 & \cosh(\theta_1 \partial/\partial\mu) \end{pmatrix},$$

where the pulse "area" is given by $\theta_1 = \kappa A_i A_i^* \Delta z$. The evolution of the electron distribution in the drift regions is governed by matrices generating rotations about the w_3 axis, exactly as in the conventional photon echo. When one calculates (w_1, w_2, w_3) at positions $z > z_1 + \Delta z$ by evaluating a product of matrices acting on the initial distribution at $z = 0$, one finds that at most positions dephasing leads to rapid oscillations in w_1 and w_2. Thus the RHS of Eq. (3) is very small. However, at $z = 2z_1$, a rephasing occurs such that

$$\int g_1(2z_1, \mu)\, d\mu = -\sin^2(\tfrac{1}{2}\theta_1 z_1) \int g_1^*(0, \mu)\, d\mu. \quad (9)$$

Thus Eq. (3) indicates that an echo pulse of laser radiation will be produced at $z = 2z_1$ if a third magnet section is located there. The strongest echo is expected if $\theta_1 z_1 = \pi$.

The free-electron echo might be useful in schemes to increase the efficiency of the FEL by recirculating the electron beam around a storage ring. In this case we consider wrapping the z coordinate around the ring, so that the magnets at $z = 0$ and $z = 2z_1$ are physically the same. Further study of such possibilities is underway.

B.5. The High-Power Cyclotron Maser (Invited), V. GRANATSTEIN, *Naval Research Laboratory, Washington, D. C. 20375.* (30 min.)

The cyclotron maser has produced record power levels at cyclotron wavelengths of 1–3 mm. Peak powers of hundreds of megawatts have been produced in short pulses, and quasi-cw devices with outputs of hundreds of kilowatts are under development.

B.6. Development of a Cerenkov Light Source, JOHN SHEPPARD, G. B. ROTHBART, M. A. PIESTRUP, R. A. POWELL, AND R. H. PANTELL, *Stanford University, Dept. of Electrical Engineering, Stanford, Calif. 94305,* AND R. A. GEARHART, *Stanford Linear Accelerator Center, Stanford, Calif. 94305.* (15 min.)

We have developed and are testing a unique source of intense vacuum ultraviolet (vuv) radiation where, prior to this time, few radiation sources in this portion of the spectrum existed, particularly for wavelengths shorter than 1100 Å. This source takes advantage of the Cerenkov effect, together with a novel optical geometry that allows the entire Cerenkov cone of a single frequency to be collected and focused to a point.

Generation of Cerenkov radiation is accomplished by allowing the 10–21 GeV primary electron beam at the Stanford Linear Accelerator Center (SLAC) to pass through a 7 m cell filled with helium at pressures of 4–400 Torr.

The forward cones of radiation are incident upon a specially designed mirror which selects and point focuses only cones of a 7 mrad opening angle. The focal plane is located 21.74 m from the mirror at a point outside the accelerator.

Since helium is dispersive at any given pressure, only one wavelength will be generated at the correct cone angle to be focused. By pressure selection, therefore, any frequency can be brought to a focus without the use of a monochrometer.

A computer code has been written to assist in a search for optimum design parameters, and to predict flux and spectral purity versus wavelength. Calculations indicate peak intensities in the range of 4–80 W/m^2 from 600 to 2000 Å/mA of primary beam current. Expressed in numbers of photons, we expect 0.5–50 $\times 10^{14}$ photons/s during the 1.6 μs beam spill, or time averaged fluxes of 0.08–8 $\times 10^{10}$ photons/s. This compares favorably to synchrotron sources in terms of optical output that is delivered to the experimeter.

Spectral purity is achieved by using a 2.8-mm-diam iris at the focus. Bandwidth can be as small as 0.1% at 600 Å, and is about 20% at 2000 Å.

First tests of this system (called CHURP) were made during the winter running cycle at SLAC using an air medium and observing the properties of the visual radiation. In this system, all physical parameters are well known and afford the opportunity of accurately checking experimental results.

As the pressure of air is increased from 45 to 85 Torr, concentric rings of light are observed to diminish in diameter to a focus and then reappear as rings of increasing diameter. By observing the dependence of the ring diameter upon pressure, and the pressure for which light is focused, the geometrical characteristics of the system are fully measured. Our data show that the expected optical properties of collection angle and focal length are correct to within experimental error (±0.4%).

The distribution of light at the focus and focal size have been measured using a linear photodiode scanning array. The distribution is triangular with a FWHM = 2.8 mm.

The total output power of the system versus cell pressure has been measured and compared with theory. The near-linear dependence of power upon pressure is observed to within ±7%, and the absolute power observed agrees with theoretical calculations to within 6%. Accuracy can be substantially enhanced by careful calibration of the beam current monitors (toroids) and correcting data for small long-term drifts in beam current.

Finally, the radial polarization of the Cerenkov ring has been observed, and polarization >0.965 has been measured.

Results using helium and for vuv output will be presented, and several immediate applications will be discussed.

B.7. The Operation Regimes of Cerenkov, Smith-Purcell and TW Amplifiers, AVRAHAM GOVER, *Tel-Aviv University School of Engineering, Tel-Aviv, Israel.* (15 min.)

The interaction of an electron beam with a guided mode in a slow-wave structure is analyzed in a general way using Maxwell and Boltzmann equations and assuming initial conditions as the entrance to the slow waveguide. The cases of a dielectric waveguide (Cerenkov amplifier) and of periodic waveguide [Smith-Purcell laser, TW (traveling wave) amplifier] are shown to be equivalent, and their gain expressions are presented and discussed in comparison to previous derivations.[1-3]

In the high electron density regime $\lambda \gg \lambda_D$ (λ_D is the Debye wave number) we are in the collective regime and our expressions reduce to the TWT (traveling wave tube) equations. Particularly near synchronism the gain g relates to the electron density n_0 as

$$g \propto n_0. \quad (1)$$

In the opposite regime ($\lambda \ll \lambda_D$) we are in the single-electron interaction regime and we have

$$g \propto n_0. \quad (2)$$

We also distinguish between the long interaction length (inhomogeneous broadening) regime where $\lambda/l \ll v_{th}/v_0$ and the opposite regime (homogeneous broadening) where $\lambda/l \gg v_{th}/v_0$. Here l is the interaction length, v_0 is the beam velocity, and v_{th} is the beam velocity spread. In the first case

$$g \propto n_0 f'(\omega/\beta_1), \quad (3)$$

where $f'(v)$ is the derivative of the electron velocity distribution function, and ω/β_1 is the phase velocity of the slow electromagnetic wave. In the second case the gain is not exponential and behaves like

$$g \propto n_0 \frac{d}{d\eta} \frac{\sin^2\eta}{\eta^2}, \quad (4)$$

where

$$\eta \equiv \frac{1}{2}\left(\frac{\omega}{\beta_1} - v_0\right)\frac{\beta_1 l}{v_0}, \quad (5)$$

similarly to the bremsstrahlung free-electron laser.[4] This expression applies only as long as

$$\omega/\beta_1 - v_0 \gg v_{th}.$$

629

Operation of Cerenkov and Smith-Purcell free-electron laser amplifiers and laser oscillators is then considered in the various operational regimes. Design considerations for the operation of such devices in the FIR wavelength regime are presented including considerations of waveguide optimization with regard to low losses and high-interaction impedance.

Finally, late results will be presented on the analysis of new kinds of free-electron lasers based on periodic modulation of a longitudinal electric field.

[1]A. Gover, A. Yariv, and P. Yeh, Eighth International Conference on Quantum Electronics, Opt. Commun. 18, 222 (1976); A. Gover and A. Yariv, Appl. Phys. (to be published).
[2]F. S. Rusin, High Power Electronics (in Russian) 5, 9 (1968).
[3]J. E. Walsh, T. C. Marshall, and S. P. Schlesinger, IEEE Trans. MIT-25, 561 (1977).
[4]F. A. Hopf, P. Meystre, M. O. Scully, and W. H. Louisell, Phys. Rev. Lett. 47, 1215 (1976).

Session C

Monday, May 29, 1978

8:30 A.M. Grand Ballroom D

Solid-State Lasers, Optical Materials, Detectors, and Devices

Presider: R. E. Palmer

C.1. Lasing and Fluorescence in $K_5NdLi_2F_{10}$

A. LEMPICKI AND B. MCCOLLUM,* *GTE Laboratories, Inc., Waltham, Mass. 02154,* AND S. R. CHINN AND H. Y.-P. HONG,† *Lincoln Laboratory, Massachusetts Institute of Technology, Lexington, Mass. 02173.* (15 min.)

We have synthesized a new Nd compound, $K_5NdLi_2F_{10}$, and have measured some of the lasing and fluorescence properties of Nd^{3+} in this material. This is the first stoichiometric Nd fluoride in which stimulated emission has been obtained, and a comparison of its characteristics with those of the recently investigated stoichiometric Nd oxides (such as NdP_5O_{14}) may provide information on some of the important energy transfer and relaxation mechanisms in these high-Nd-concentration materials.

Crystals were grown from a charge of NdF_3:9 LiF:6 KF in a closed graphite crucible in an argon atmosphere. After equilibration at 900 °C for several hours, the charge was slowly cooled to room temperature, and small crystal platelets were manually separated from the flux matrix.

The structure and thus the composition of the crystals were determined by using the single-crystal x-ray heavy-atom method. (Now that the composition of the new material has been found, it is likely that improved crystal growth can be achieved by using a growth charge of this same composition.) The space group is orthorhombic, Pnma, with lattice constants $a = 20.6519$ Å, $b = 7.7787$ Å, and $c = 6.9017$ Å. The Nd point symmetry is m, with eightfold coordination to surrounding F^- ions. The Nd^{3+} concentration is 3.61×10^{21} cm^{-3}, and the smallest Nd-Nd separation is 6.73 Å.

Fluorescence and lasing data were taken with a platelet $0.3 \times 0.8 \times 0.1$ mm, with the a axis (the lasing direction) perpendicular to the broad face. The $^4F_{3/2} \rightarrow {}^4I_{9/2}$, $^4I_{11/2}$ fluorescence spectra were obtained at 300, 70, and 2 K, using cw excitation from a rhodamine-6G dye laser to pump the 580 nm Nd^{3+} absorption band. At room temperature, the $^4F_{3/2} \rightarrow {}^4I_{11/2}$ emission consists of six well-resolved broad peaks, with the two strongest at 1048 and 1052 nm, having full widths ~25 cm^{-1}. At low temperatures, the emission lines become quite narrow, indicating that the room-temperature broadening is homogeneous. Although the low Nd site symmetry m does not impose any selection rules, changes in relative intensity among the components are observed in different polarizations. The low-temperature $^4F_{3/2}$ splitting is 50 cm^{-1}, decreasing slightly to 45 cm^{-1} at room temperature. The fluorescent lifetime of the $^4F_{3/2}$ manifold was measured using pulsed excitation in the 800 nm Nd^{3+} absorption band. The lifetime increased smoothly from 300 μs at room temperature to 640 μs at 2 K. This is in striking contrast to the behavior of NdP_5O_{14} (NPP), in which the lifetime is independent of temperature.

Lifetime measurements were also made on polycrystalline samples containing Ce as well as Nd, which were prepared by a different technique. X-ray diffraction analysis showed that these samples contained some amounts of a $KNd_xCe_{1-x}F_4$ phase, but data obtained using spectral discrimination of the emission wavelength indicated that the lifetime of the $K_5Nd_yCe_{1-y}Li_2F_{10}$ phase changed little with Nd concentration over a considerable range of y (qualitatively estimated from the starting charge composition). Both the temperature dependence and the preliminary concentration quenching behavior indicate that the energy migration and cross-relaxation processes may be significantly different in KNLF than in the stoichiometric Nd oxides.

Laser emission was obtained with the platelet sample in the center of a nearly concentric 10-cm-long resonator. Collinar pumping by a chopped cw dye laser (λ 586 nm) was used, with approximately 40% of the pump radiation absorbed in the 98-μm-thick sample. The lowest threshold absorbed power was 1.4 mW, with a 0.2% transmitting output mirror. With an output transmission of 1%, the threshold power increased to 2.1 mW, and a 19% slope power efficiency was measured. Using a value for the internal round-trip loss of ~2% (calculated from the slope efficiency), we can compare the performance of KNLF with NPP under the same experimental conditions. Taking typical NPP laser parameters measured previously, we estimate that the product of the KNLF effective cross section and lifetime $\sigma\tau$ is roughly 1.2 times that of NPP. The effective ($^4F_{3/2}$ population-weighted) cross section for KNLF at a wavelength of 1048 nm is about 0.8×10^{-19} cm^2. At higher pump levels, emission at 1052 nm was observed, polarized orthogonally to the 1048 nm emission. Lasing was also observed with the sample mounted at Brewster's angle, but with higher threshold.

With its relatively long spontaneous fluorescent lifetime, KNLF may be an attractive candidate for miniature pulsed laser devices in which Q-switched operation is enhanced by efficient energy storage in the laser material. One factor contributing to the long lifetime may be the large separation between nearest-neighbor Nd^{3+} ions.

*Work partly supported by the Army Research Office, Durham, N.C.
†The Lincoln Laboratory portion of this work was supported by the Department of the Air Force.

C.2. Efficient cw Optically Pumped $Ni:MgF_2$ Laser,*

P. F. MOULTON AND A. MOORADIAN, *Lincoln Laboratory, Massachusetts Institute of Technology, Lexington, Mass. 02173.* (15 min.)

Electronic energy levels of transition-metal ion impurities in host crystals such as MgF_2 are, in general, strongly coupled to phonons, which means they can have large fluorescence linewidths, appreciable Stokes shifts between absorption and emission, and broad absorption bands that permit pumping by available cw lasers. These characteristics allow cw, tunable, four-level laser operation in a manner analogous to cw dye and F-center lasers. Of particular interest is Ni^{2+}-doped MgF_2($Ni:MgF_2$), in which the laser operation with lamp excitation was first reported in 1963.[1] In the present work, the $^3A_{2g} \rightarrow {}^3T_{2g}$ transition of $Ni:MgF_2$ has been optically pumped with a cw, 1.33 μm Nd:YAG laser, and lasing has been observed from the same transition in the 1.6–1.8 μm region.

The laser crystal used in these experiments was cut from a MgF_2 boule containing 0.4-wt % Ni, which was grown by a vertical gradient-freeze technique.[2] The crystal was a 5 × 5 mm square rod, 2 cm long. One end of the rod was polished flat and coated for high transmission at 1.33 μm and high reflection between 1.6 and 1.8 μm; the other end was polished to a convex surface with a 2 cm radius to form a confocal cavity and was coated for >99% reflectivity from 1.6 to 1.8 μm. The laser rod was held by a spring-loaded clamp to a copper heat sink in a helium-gas-cooled variable-temperature Dewar. Pumping geometry was collinear and the pump beam, focused to a measured beam radius of 220 μm in the TEM_{00}, entered the $Ni:MgF_2$ crystal through the flat face.

Threshold absorbed pump power and operating wavelength of the $Ni:MgF_2$ laser were measured with a TEM_{00} pump beam as a function of heat-sink temperature from 20 to 200 K. Threshold power increased from 50 mW at low temperature to 180 mW at 200 K. Operating wavelength tuned from 1.632 to 1.634 μm between 20 and 90 K, jumped to 1.730 μm at 100 K and increased slowly from that point to 1.750 μm at 200 K. The laser output spectrum near the threshold at 80 K showed a total of four modes oscillating over a region about ¾ cm^{-1} wide.

Figure 1 shows the output power as a function of absorbed pump power. The heat-sink temperature was 20 K at low pump levels but rose to 35 K at the highest pump power because of the limited cooling capacity of the Dewar; output wavelength was ~1.63 μm. To obtain absorbed power levels above 200 mW, the pump power was increased by increasing the number of transverse modes. The increase in slope efficiency apparent in

630

MARON

JOURNAL
of the
OPTICAL SOCIETY
of
AMERICA

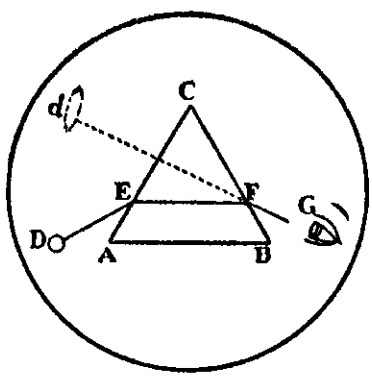

MAY
1978

VOLUME 68 NUMBER 5